Optics Communications 393 (2017) 152–155

Contents lists available at ScienceDirect

Optics Communications

journal homepage: www.elsevier.com/locate/optcom

Frequency-doubled telecom fiber laser for a cold atom interferometer using optical lattices

Fabien Theron[a], Yannick Bidel[a,*], Emily Dieu[a], Nassim Zahzam[a], Malo Cadoret[a,b], Alexandre Bresson[a]

[a] ONERA - The French Aerospace Lab, BP 80100, 91123 Palaiseau Cedex, France
[b] Laboratoire Commun de Métrologie, CNAM, 61 rue du Landy, 93210 La Plaine Saint-Denis, France

ARTICLE INFO

Keywords:
Atom interferometry
Optical lattice
Second harmonic generation
Telecom fiber laser
Rubidium

ABSTRACT

A compact and robust frequency-doubled telecom laser system at 780 nm is presented for a rubidium cold atom interferometer using optical lattices. Adopting an optical switch at 1.5 μm and a dual-wavelength second harmonic generation system, only one laser amplifier is required for the laser system. Our system delivers a 900 mW laser beam with a detuning of 110 GHz for the optical lattice and a 650 mW laser beam with an adjustable detuning between 0 and −1 GHz for the laser cooling, the detection and the Raman transitions.

1. Introduction

Cold atom interferometers [1] have proven to be accurate and sensitive sensors to measure gravity acceleration [2–4], gravity gradients [5,6] and rotation [7,8]. Experiments using optical lattices [9] are increasingly being conducted to improve the performance of these sensors. Indeed, optical lattices allow the precise control of the momentum of the atoms, and therefore their movement. It is, therefore, possible to levitate atoms with a well controlled force in order to build a compact gravimeter with levitating atoms [10,11]. It is also possible to increase the momentum transfer in an atomic splitter and thus to increase the sensitivity of the sensor [12–14]. Optical lattices can also be used to impart a well controlled velocity to the atoms, which is particularly important for gyroscopes or large atomic fountain experiments [15]. Finally optical lattices can be used to separate and transport a cold atom cloud in order to build a sensor with spatially separated clouds of cold atoms to allow the measurement of gravity gradients [16]. The disadvantage of using optical lattices in atom interferometry sensors is the requirement of another laser, generally detuned around 100 GHz from the atomic transition with a power of at least few hundred mW. Until now, the optical lattices were implemented with an independent laser from the one used for the atom interferometer experiment. The whole laser system for the sensor is thus more complicated, larger and less robust. The second laser has thus important impacts for the construction of a compact and robust sensor [17] for geophysics, navigation or space applications. Much research [18–20] have been undertaken over the last few years to achieve compact and robust laser systems for atom interferometers: none of these addressed the use of optical lattices, however.

In this article, we present a laser system which generates the lasers for a cold atom interferometer and optical lattices with only one laser amplifier (usually the less reliable part). Our laser system is based on a frequency doubled telecom fiber bench which addresses rubidium atoms (λ = 780 nm) and is derived from the laser system described in reference [10]. Two independent laser systems for the cold atom interferometer and for the optical lattices were adopted. Each laser system was composed of a laser source at 1.5 μm, an EDFA (Erbium Dopped Fiber Amplifier), and a second harmonic generation bench. The laser system presented in this article combines the two laser sources at 1.5 μm using an optical switch such that only one EDFA is required. This approach is possible as the optical lattice laser and the cold atom interferometer laser are not needed at the same instant. In the first part of this article, we will present the general architecture of our laser system, then we will describe the dual wavelength second harmonic generation and finally we will present the lock of the optical switch.

2. General description of the laser system

The laser system for the cold atom interferometer and the optical lattices is described on Fig. 1. The atom interferometer laser source (AI laser) which provides the frequencies for laser cooling and trapping, detection and Raman transition is an erbium fiber DFB laser at 1.5 μm (output power 20 mW, linewidth 2 kHz). This laser source is locked relative to the rubidium transitions with a detuning that can be adjusted from 0 to −1 GHz. The repumper and the second Raman

* Corresponding author.

http://dx.doi.org/10.1016/j.optcom.2017.02.013
Received 10 October 2016; Received in revised form 2 February 2017; Accepted 4 February 2017
Available online 23 February 2017

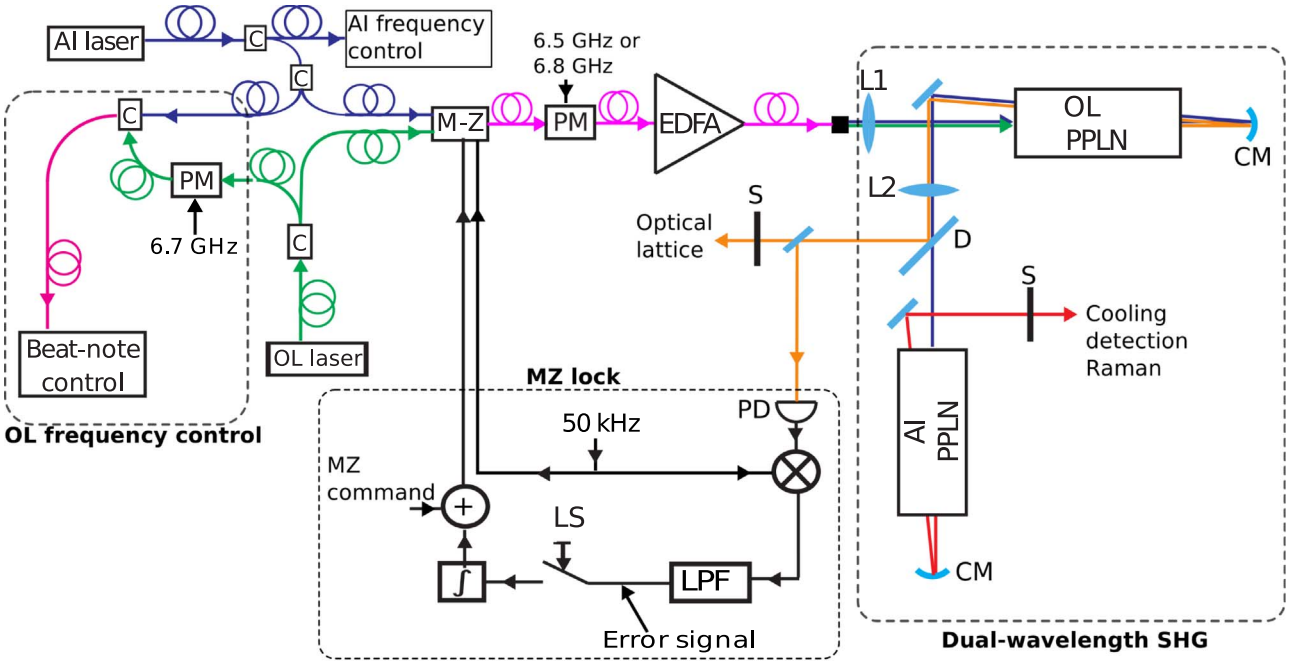

Fig. 1. Diagram of the laser system and the Mach-Zehnder lock. AI: Atom Interferometry, OL: Optical Lattice, C: coupler, PM: Phase Modulator, M-Z: Mach-Zehnder, EDFA: Erbium Doped Fiber Amplifier, L: Lens, PPLN: Periodically-Poled Lithium Niobate, D: Dichroic mirror, CM: gold Concave Mirror, S: Shutter, PD: PhotoDiode, LPF: Low Pass Filter, LS: Lock Switch.

frequency are generated using a phase modulator fed by a radio frequency at 6.5 GHz or 6.8 GHz. This part of the laser is described in detail in reference [21]. The optical lattice laser source (OL laser) is a DFB laser diode at 1.5 μm (Avanex DFB, output power: 10 mW, linewidth 1 MHz). The OL laser is detuned by 55 GHz at 1.5 μm relative to the AI laser which gives a detuning of 110 GHz at 780 nm. The detuning of the OL laser is controlled using a beat-note between the two lasers at 1.5 μm. In order to have an easily measurable beat-note at lower frequency, a phase modulator fed by a radio frequency at 6.7 GHz is put on the optical lattice path and generates sidebands separated by 6.7 GHz. For a detuning of 55 GHz at 1.5 μm, a RF signal at 1.4 GHz is measured corresponding to the beat note between the AI laser and the 8^{th} sideband of the modulated OL laser.

The AI laser and the OL laser are combined at 1.5 μm by an electro-optical modulator which acts like a continuous optical switch between each laser. This component is a wave-guided Mach-Zehnder interferometer (MZ) from EO Space with an extinction of 30 dB and a voltage required for inducing a phase change of π equal to $V_\pi = 5$ V. As the path difference in the MZ is close to zero, interference signals of OL laser and AI laser are in phase opposition, and the output of the MZ can be described by Eq. (1). Therefore, changing the MZ voltage command V allows to select the AI laser or the OL laser at the output.

$$I_{out} = I_{AI} \times \cos^2\left(\frac{\pi}{2}\cdot\frac{V}{V_\pi}\right) + I_{OL} \times \sin^2\left(\frac{\pi}{2}\cdot\frac{V}{V_\pi}\right) \quad (1)$$

Then, the laser goes through a 5 W Erbium Doped Fiber Amplifier (EDFA). In order to avoid damaging the EDFA, the input power must be constant. The power of both laser sources have therefore been adjusted to have the same power at the output of the MZ regardless of the MZ command. Finally, the laser is sent to the dual-wavelength second harmonic generation bench.

3. Dual-wavelength frequency second harmonic generation

The dual-wavelength second harmonic generation configuration is similar to the one described in reference [22]. It consists of two bulk PPLN crystals, in double-pass configuration (Fig. 1).

At the output of the EDFA fiber, the laser is focused in a first PPLN crystal using a 75 mm focal length lens (L1), and the double pass configuration is realized by a 10 cm curvature radius gold mirror (CM). At the center of the crystal, the waist of the laser is 23 μm. This first PPLN is phase matched for OL frequencies (T_{OL} = 133.45 °C) and provides an OL laser power of 900 mW at 780 nm, with an input power at 1.5 μm of 4.3 W. The measurement of the power at 780 nm versus the power at 1.5 μm is shown in Fig. 2. The experimental data are fitted by Eq. (2) in the depleted pump regime [23].

$$P_{780} = P_{1.5}\tanh^2(\sqrt{\eta P_{1.5}}) \quad (2)$$

The fit gives a conversion efficiency of η = 5.4%/W.

The dichroic mirror (D) transmits the AI laser at 1.5 μm to the second PPLN crystal, and reflects the OL laser at 780 nm. The AI laser at 1.5 μm is focused inside the second PPLN crystal using a 60 mm focal length lens (L2) in 2–2 f design, in order to get the same waist for both crystals. The double pass configuration in the crystal is achieved with a 10 cm curvature radius gold mirror. The second PPLN crystal is phase matched for AI frequencies (T_{AI} = 134 °C) to provide an AI laser power of 650 mW at 780 nm with an input power at 1.5 μm of 3.5 W. For this crystal, the fit of the power at 780 nm versus the power at 1.5 μm gives a conversion efficiency of η = 5.1%/W (see Fig. 2).

4. Effect of the finite extinction of the optical switch

Due to the finite extinction of the optical switch, the OL and the AI laser beams will be contaminated by a small fraction of light at the frequency of the other laser and at the sum frequency of the 1.5 μm AI laser and the 1.5 μm OL laser. The parasitic laser frequency which has the biggest impact on the experiment is the AI frequency in the OL laser beam because it is close to resonance and could induce extra spontaneous emission in the optical lattice. It is, therefore, important to evaluate the relative power of this parasitic laser frequency and to estimate its effects on the spontaneous emission rate. We measure an extinction of the optical switch equal to $\eta_{MZ} = 1 \times 10^{-3}$. By measuring the power at 780 nm versus the frequency of the laser for the OL crystal (see Fig. 3), the ratio between the conversion efficiency at the AI frequency and the conversion efficiency at OL frequency is equal to $\eta_{conv} = 1.5 \times 10^{-2}$. The relative power at AI frequency in the OL laser

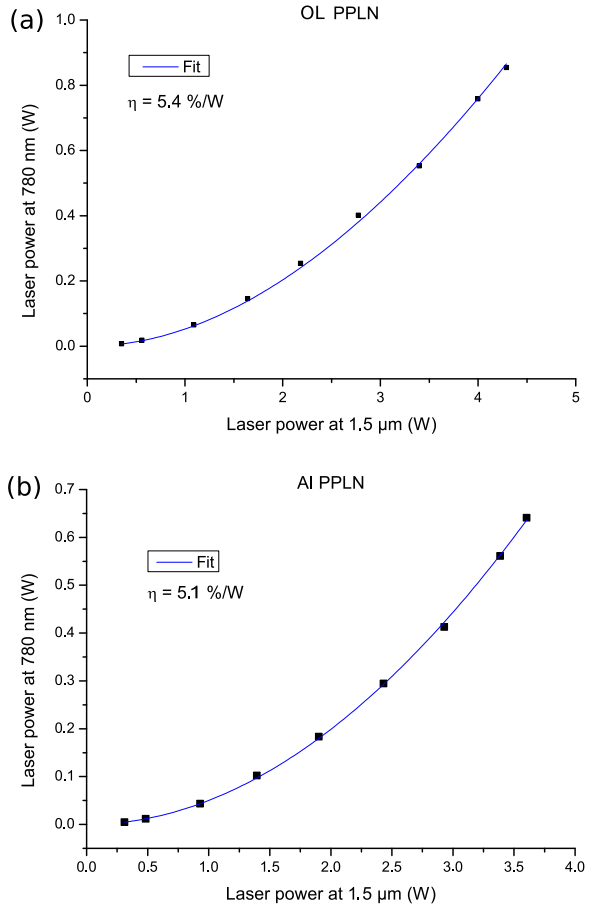

Fig. 2. Second harmonic generation power at 780 nm as a function of pump power in a double-pass configuration. Top (a) frequency doubling efficiency of the OL laser using the OL PPLN crystal. Bottom (b) frequency doubling efficiency of the AI laser using the AI PPLN crystal.

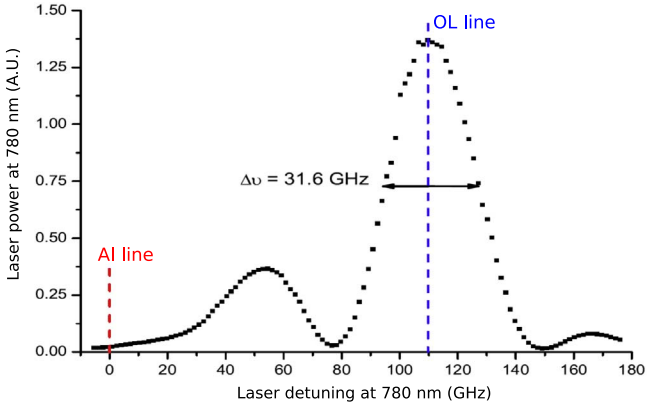

Fig. 3. Second harmonic generation at 780 nm in the PPLN phase matched for OL conversion, with 1.5 μm laser at 4.5 W. OL line in blue and AI line in red.

beams is equal to $\epsilon_{AI} = \eta_{MZ}^2 \times \eta_{conv} = 1.5 \times 10^{-8}$. During the optical lattice stage, the AI can be detuned by $\Delta_{AI} = 1$ GHz compared to the atomic resonance. Thus, the AI parasite laser line causes a spontaneous emission rate $\epsilon_{AI} \times \frac{\Delta_{OL}^2}{\Delta_{AI}^2} = 1.8 \times 10^{-4}$ less than the spontaneous emission rate caused at the OL laser line. We can conclude that the effect of AI parasitic frequency in the OL beam will be negligible.

5. Lock of the mach-zehnder optical switch

The MZ switch presents a long term drift on the time scales of hours which results in a drift of the command voltages needed to select AI and OL frequencies. A continuous correction of the MZ voltage command has thus been implemented by modulating the voltage of the MZ at 50 kHz and by detecting this modulation on the power at 780 nm of the OL beam (Fig. 1). For that purpose, a part of the OL beam is sent to a photodiode. Then the signal is amplified, demodulated at 50 kHz and low pass filtered. The error signal obtained at this point is integrated, summed to the electric command which switch from AI to OL and sent to the MZ input. As the error signal is only available when the OL frequency is selected, an electronic switch (LS) has been inserted before the integrator in order to activate the lock only during the optical lattice stage. During the AI stage, the output of the integrator will thus stay at a constant value. This non-correction of the drift of the MZ during the AI stage is acceptable because the duration of this step is very short (~1 s) compared to the time scale of the drift of the MZ (few hours).

6. Conclusion

We have developed a compact and robust laser system for a cold atom interferometry sensor using optical lattices. The association of a fibered Mach-Zehnder electro-optical switch and a dual-wavelength second harmonic generation unit has allowed the use of only one laser amplifier and thus led to a laser system which is more reliable, more compact and with lower electrical consumption. We have checked that the finite extinction of the switch does not cause additional spontaneous emission in the optical lattice. A power of 650 mW for the cold atom interferometer and 900 mW for the optical lattice have been obtained. These laser powers can be increased by using a 10 W laser amplifier, which is commercially available. By taking parameters of the dual-wavelength architecture and using Eq. (2), one obtains an OL laser power of 3 W, and an AI laser power of 2 W. The laser system presented in this article demonstrates that an atomic sensor, with enhanced performance using optical lattice technology, can have applications in space technology, geophysics or navigation.

Acknowledgements

We thank F. Nez, from the Laboratoire Kastler Brossel (LKB), for his help on the project. We acknowledge funding support from the Direction Scientifique Générale of ONERA and the Direction Générale de l'Armement (DGA).

References

[1] G.M. Tino, M.A. Kasevich, Atom Interferometry, in: Proceedings of the International School of Physics Enrico Fermi, Course CLXXXVIII (IOS Press, Amsterdam, 2014).
[2] A. Peters, K.Y. Chung, S. Chu, Metrologia 38 (2001) 25.
[3] P. Gillot, O. Francis, A. Landragin, F. Pereira dos Santos, S. Merlet, Metrologia 51 (2014) 15.
[4] Z.K. Hu, B.L. Sun, X.C. Duan, M.K. Zhou, L.L. Chen, S. Zhan, Q.Z. Zhang, J. Luo, Phys. Rev. A 88 (2013) 043610.
[5] J.M. McGuirk, G.T. Foster, J.B. Fixler, M.J. Snadden, M.A. Kasevich, Phys. Rev. A 65 (2002) 033608.
[6] F. Sorrentino, Q. Bodart, L. Cacciapuoti, Y.-H. Lien, M. Prevedelli, G. Rosi, L. Salvi, G.M. Tino, Phys. Rev. A 89 (2014) 023607.
[7] T.L. Gustavson, P. Bouyer, M.A. Kasevich, Phys. Rev. Lett. 78 (1997) 2046.
[8] A. Gauguet, B. Canuel, T. Lévèque, W. Chaibi, A. Landragin, Phys. Rev. A 80 (2009) 063604.
[9] J.H. Denschlag, J.E. Simsarian, H. Haffner, C. McKenzie, A. Browaeys, D. Cho, K. Helmerson, S.L. Rolston, W.D. Phillips, J. Phys. B 35 (2002) 3095.
[10] R. Charrière, M. Cadoret, N. Zahzam, Y. Bidel, A. Bresson, Phys. Rev. A 85 (2012) 013639.
[11] M. Andia, R. Jannin, F. Nez, F. Biraben, S. Guellati-Khélifa, P. Cladé, Phys. Rev. A 88 (2013) 031605.
[12] S. Chiow, T. Kovachy, H.-C. Chien, M.A. Kasevich, Phys. Rev. Lett. 107 (2011) 130403.
[13] H. Müller, S. Chiow, S. Herrmann, S. Chu, Phys. Rev. Lett. 102 (2009) 240403.
[14] G.D. McDonald, C.C.N. Kuhn, S. Bennetts, J.E. Debs, K.S. Hardman, M. Johnsson, J.D. Close, N.P. Robins, Phys. Rev. A 88 (2013) 053620.
[15] S.M. Dickerson, J.M. Hogan, A. Sugarbaker, D.M.S. Johnson, M.A. Kasevich, Phys.

Rev. Lett. 111 (2013) 083001.
[16] O. Carraz, C. Siemes, L. Massotti, R. Haagmans, P. Silvestrin, Microgravity Sci. Technol. 26 (2014) 139–145.
[17] Y. Bidel, O. Carraz, R. Charrière, M. Cadoret, N. Zahzam, A. Bresson, Appl. Phys. Lett. 102 (2013) 144107.
[18] O. Carraz, F. Lienhart, R. Charrière, M. Cadoret, N. Zahzam, Y. Bidel, A. Bresson, Appl. Phys. B 97 (2009) 405–411.
[19] M. Schmidt, M. Prevedelli, A. Giorgini, G.M. Tino, A. Peters, Appl. Phys. B 102 (2011) 11–18.
[20] P. Cheinet, F. Peirera dos Santos, T. Petelski, J. le Gouët, J. Kim, K.T. Therkildsen, A. Clairon, A. Landragin, Appl. Phys. B 84 (2006) 643–646.
[21] F. Theron, O. Carraz, G. Renon, N. Zahzam, Y. Bidel, M. Cadoret, A. Bresson, Appl. Phys. B 118 (2015) 1–5.
[22] V. Ménoret, R. Geiger, G. Stern, N. Zahzam, Y. Bidel, B. Battelier, A. Bresson, A. Landragin, P. Bouyer, Opt. Lett. 36 (2011) 4128–4130.
[23] D.R. White, E.L. Dawes, J.H. Marburger, IEEE J. Quantum Electron. QE-6 (1970) 793–796.